Dalton Transactions

PAPER

View Article Online
View Journal | View Issue

Cite this: *Dalton Trans.*, 2017, **46**, 9192

Structure stability of HKUST-1 towards water and ethanol and their effect on its CO_2 capture properties†

J. Raziel Álvarez,[a] Elí Sánchez-González,[a] Eric Pérez,[a] Emilia Schneider-Revueltas,[b] Ana Martínez,[b] Adriana Tejeda-Cruz,[b] Alejandro Islas-Jácome,*[c] Eduardo González-Zamora*[c] and Ilich A. Ibarra*[a]

Received 20th May 2017,
Accepted 20th June 2017

DOI: 10.1039/c7dt01845b

rsc.li/dalton

Water and ethanol stabilities of the crystal structure of the Cu-based metal–organic framework (MOF) HKUST-1 have been investigated. Vapour (water and ethanol) sorption isotherms and cyclability were measured by a dynamic strategy. The ethanol sorption capacity of HKUST-1 at 303 K remained unchanged contrasting water sorption (which decreased along with the sorption experiment time). Considering the binding energy of each sorbate with the open Cu(II) sites, obtained by the use of diffusion coefficients, we showed the superior crystal stability of the HKUST-1 framework towards ethanol. Finally, a small quantity of ethanol (pre-adsorbed) slightly enhanced CO_2 capture without crystal structure degradation.

Introduction

Metal–Organic Frameworks (MOFs) are crystalline materials consisting of metal ions and organic bridging ligands with potential voids.[1] MOFs have emerged as excellent candidates for selective carbon dioxide capture due to their modular structure, high porosity, large surface area and chemical tunability.[2,3] Nevertheless, the industrial deployment of MOFs as solid adsorbents for CO_2 capture and sequestration (CCS) is delimited by their hydrothermal stability.

In all industrial CO_2 capture technologies, water vapour takes part, in an intrinsic or extrinsic way, in the design of the CCS process.[4–6] Water stability is an important issue due to possible MOF structure degradation by hydrolysis or ligand displacement.[7,8] Water vapour also can considerably reduce the CO_2 uptake as a result of high competition for preferential adsorption sites within MOFs.[9,10] Although these are very well-known and studied characteristics, recently the advantages of water inclusion and its key role in the physicochemical interactions for CO_2 capture within the porous structure of MOFs have been demonstrated.[11,12] Indeed, the control of pre-adsorbed water can enhance CO_2 capture in some MOFs,[13] such as InOF-1,[14] MIL-53(Al),[15] NOTT-400[16] and NOTT-401.[17]

HKUST-1 (HKUST = Hong Kong University of Science and Technology), first synthesized in 1999, is an MOF with the formula $[Cu_3(BTC)_2(H_2O)_3]_n$ (BTC = benzene-1,3,5-tricarboxylate) constructed by square Cu_2 paddlewheel clusters connected by BTC ligands forming a cF crystal structure with $Fm\bar{3}m$ symmetry.[18] HKUST-1 has a rigid porous open-framework with bimodal pore size distribution and is one of the most studied MOFs that exhibits unsaturated metal sites (open metal sites).[19,20]

The sorption properties of HKUST-1 have been investigated extensively.[21–23] Water uptake in the HKUST-1 has been experimentally[24–26] and computationally[27,28] studied. This material is extremely sensitive to water content with a total water vapour uptake of 32 mmol g^{-1} at 298 K and 90% relative humidity (RH).[29] Due to the very strong interaction between open Cu(II) sites (the coordinatively unsaturated sites from the copper paddlewheel) and water molecules, the crystal structure of HKUST-1 suffers an irreversible degradation when it is continuously exposed to water in a liquid or vapour form.[26,30] Additionally, this degradation process decreases, considerably, the gas sorption capacity of this material.[31] Nevertheless, the same behaviour is not true for other polar sorptives.[23]

[a]*Laboratorio de Fisicoquímica y Reactividad de Superficies (LaFReS), Instituto de Investigaciones en Materiales, Universidad Nacional Autónoma de México, Circuito Exterior s/n, CU, Del. Coyoacán, 04510, Ciudad de México, Mexico. E-mail: argel@unam.mx*
[b]*Instituto de Investigaciones en Materiales, Universidad Nacional Autónoma de México, Circuito Exterior s/n, CU, Del. Coyoacán, 04510, Ciudad de México, México*
[c]*Departamento de Química, Universidad Autónoma Metropolitana-Iztapalapa, San Rafael Atlixco 186, Col. Vicentina, Iztapalapa, C. P. 09340, Ciudad México, Mexico. E-mail: egz@xanum.uam.mx, aij@xanum.uam.mx*

†Electronic supplementary information (ESI) available: Supplementary figures and additional characterization. See DOI: 10.1039/c7dt01845b

The CO_2 sorption properties of HKUST-1 have been extensively studied due to the great affinity of its open Cu(II) sites to CO_2 molecules.[21,32] CO_2 uptakes (on HKUST-1) have shown to be dependent on the synthetic method and solvent exchange process,[33,34] with a maximum adsorption capacity of 14 mmol g^{-1} at 303 K and 40 bar.[35]

However, only a few studies have described the water co-adsorption with CO_2 in this MOF.[10] Moreover, the realistic flue gas streams (depending on the fuel source) consist of 5 to 7% by volume in water.[36] In HKUST-1, small quantities of pre-adsorbed water (4 wt% at 298 K) and low pressure ranges enhance slightly the CO_2 uptake in comparison with the dehydrated sample.[37,38]

Investigations of the potential use of adsorbed alcohols, for different applications in MOFs, have recently increased.[35,38] The pre-adsorption of alcohols in MOFs for CCS applications has only been reported recently.[39] Our research group demonstrated that the pre-adsorption of ethanol,[39] methanol,[40] isopropanol[40] and *N*,*N*-dimethylformamide[41] can significantly enhance CO_2 capture in the titled microporous MOF materials. HKUST-1 exhibits high alcohol loadings at 323 K, with uptakes of 5 mmol g^{-1} for 1-hexanol to 17 mmol g^{-1} for methanol.[23,42] Nevertheless, the investigation of alcohol co-adsorptions to enhance CO_2 capture in HKUST-1 has not been performed until now. Herein, we studied the water and ethanol stability of HKUST-1 and the relationship between the pre-adsorption of these solvents with CO_2 sorption performance.

Experimental

Materials

HKUST-1 (known as copper benzene-1,3,5-tricarboxylate, Cu-BTC, MOF-199 or Basolite™ C300) was purchased from Sigma-Aldrich (lot #STBC4614 V). Ethanol (anhydrous A.C.S. reagent) was purchased from Baker and was used as received. Carbon dioxide and nitrogen (99.9% and 99.998%, respectively) were supplied by Praxair. Ethanol-impregnated HKUST-1 samples were first activated for 2 h at 423 K under vacuum and then cooled down to 303 K. Immediately, the samples were transferred to an evaporator/saturator containing ethanol at room temperature until the samples were fully saturated.

Kinetics CO_2 adsorption experiments

In order to investigate the CO_2 adsorption properties of the ethanol-impregnated HKUST-1 samples, kinetics uptake experiments were conducted using a thermobalance (Q500 HR, TA Instruments) at 303 K with a constant CO_2 gas flow rate of 60 sccm (mL min^{-1}). Water co-adsorption followed by CO_2 adsorption experiments were carried out using a dynamic water vapour sorption analyser (Q5000 SA, TA Instruments) at 303 K with a constant CO_2 flow (60 sccm) on activated samples (423 K for 2 h and under vacuum) of HKUST-1.

Dynamic vapour sorption isotherms

Water and ethanol sorption isotherms and cyclability were measured at 303 K using a gravimetric method in a DVS Advantage 1 from Surface Measurement System, UK. This instrument consists of a Cahn microbalance (mass sensitivity: 0.1 μg), with a digital optical microscope, set in an exactly controlled temperature and vapour pressure chamber (accuracy: 0.1 K and 0.7% P/P_0, respectively). Dry, high-purity nitrogen was used as a carrier gas.

Solvent stability determination

To assess the framework stability towards solvents, HKUST-1 samples were activated and exposed to water and ethanol (vapour and liquid) for 216 h. After that, HKUST-1 samples were structurally characterised.

Crystal structure

Powder X-ray diffraction (PXRD) patterns were collected in Bragg–Brentano geometry with Cu-$K_{\alpha 1}$ radiation (λ = 1.540562 Å) in a Rigaku ULTIMA IV with a nickel filter. The powder patterns were recorded from 2 to 40° (2θ) in 0.02° steps and a scan rate of 0.05° min^{-1}.

Morphology

The morphology was determined by scanning electron microscopy (SEM) using a JEOL 7600 model microscope.

Computational studies

Calculations related to geometry optimisations and single point calculations were undertaken by implementing Gaussian 09.[43] The geometry of the model was fully optimised at the B3LYP/LANL2DZ level.[44,45] Harmonic analyses were performed and local minima were identified (zero negative values).

Results and discussion

Crystal structure performance

The crystallinity of HKUST-1 was evaluated by PXRD. In Fig. 1, it is possible to observe the characteristic Bragg reflections at small 2θ angles for HKUST-1 ($2\theta \approx 6.5°$, 9.5°, 11.5° and 13.4°)[26] (Fig. 1). Additionally, the PXRD pattern confirms the high purity of HKUST-1 without any indication of Cu, CuO or

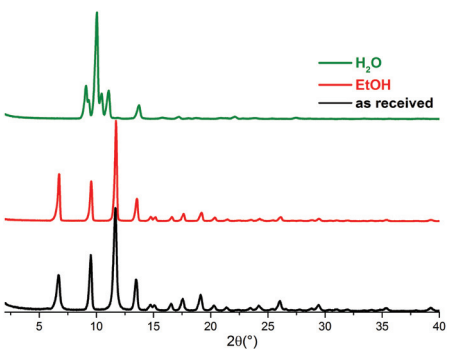

Fig. 1 PXRD comparison of the HKUST-1 sample as received (black), exposed to liquid ethanol (red) and exposed to liquid water (green) for 216 h.

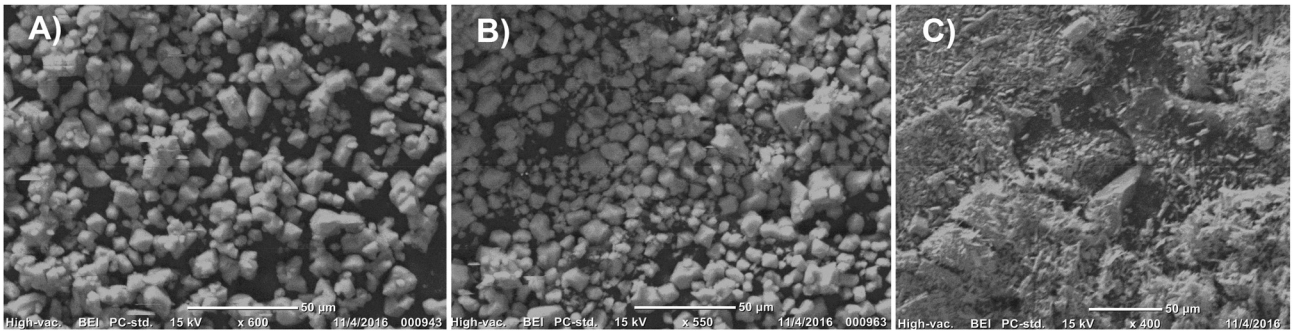

Fig. 2 Scanning electron micrograph of HKUST-1 (A) as received, (B) exposed to liquid ethanol and (C) exposed to liquid water for 216 h.

Cu_2O (the most common impurity phases).[20] The BET surface area of HKUST-1 was equal to 1809 $m^2\ g^{-1}$. As previously described,[29,30,46] the crystal structure of HKUST-1 is unstable when exposed to water. In direct contact with liquid water, the evolution of crystal degradation is quickly completed in only a few hours (Fig. S1, ESI†). However, HKUST-1 samples exposed to ethanol (liquid or vapour) did not disturb the crystal structure as confirmed by PXRD (Fig. S2, ESI†).

The reflections in the PXRD pattern of HKUST-1 exposed to liquid water do not reveal the presence of phases like $Cu(OH_2)$ or any trace of the BTC ligand. This suggested that the degradation of the crystalline structure of HKUST-1 did not involve the complete collapse of the framework, as was elegantly demonstrated by Pérez-Ramírez.[47] The BET surface area of this material showed a lower porosity of 940 $m^2\ g^{-1}$.

SEM images of the as-received HKUST-1 sample (Fig. 2a) showed a double-sided pyramidal shape with sharp edge morphology of the crystals and sizes from 2 µm to 20 µm. This homogenous morphology distribution is in good relationship with the PXRD results and confirmed the high crystallinity of the HKUST-1 sample. After liquid water exposure, needle-shaped crystals of HKUST-1 exhibited crystal-morphology degradation (see Fig. 2c). However, when the HKUST-1 was immersed in liquid ethanol, the crystal-morphology was not altered and crystal sizes similar to the as-received HKUST-1 sample were observed (see Fig. 2b).

To evaluate the vapour sorption (water and ethanol) stability of the HKUST-1 framework, samples were exposed to multiple vapour adsorption/desorption cycles at 303 K. The sorption capacities of the material once exposed to the continuous flow of water vapour decreased continuously from the first cycle to the last one (eighth cycle) (Fig. 3). The maximum water adsorption capacity for HKUST-1 decreased continuously from 65.4 to 42.9 wt% over only eight cycles.

The irreversibility of the adsorption–desorption process is in good agreement with the poor water stability of HKUST-1.[26,30]

Additionally, it is well established that the colour variation of HKUST-1, due to d–d transitions, strongly relies on the chemical environment around the Cu(II) paddlewheels, from dark violet (open Cu(II)-coordination state) to turquoise (water coordinated state).[26,48,49] In this case, the framework structure

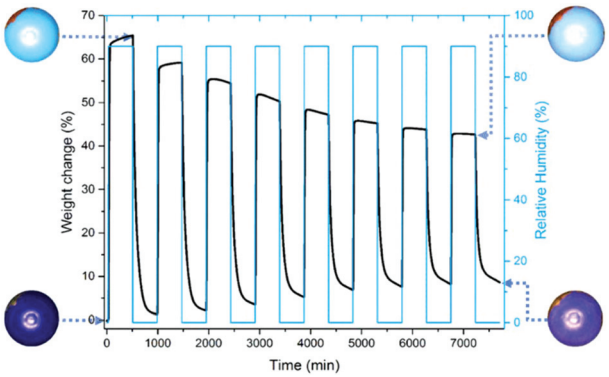

Fig. 3 Weight change variation through water sorption cycle measurements at 303 K. Inset: *In situ* optical microscope images for representative colour changes of HKUST-1 in different steps of the cycle.

degradation is well correlated with the modification of colour along with each step of adsorption–desorption cycles of water.[26]

The vapour ethanol stability was established with a continuous ethanol adsorption–desorption experiment conducted by eight cycles (Fig. 4). The maximum ethanol uptake was equal to 44.9 wt% which remained constant through all sorption cycles. Even though a concentration (strictly speaking a chemical potential) gradient is not enough to release all the strongly adsorbed ethanol molecules that remained in the adsorbed phase of HKUST-1 framework (22.1 wt%), the sorption capacities of the material remained intact over eight cycles of ethanol adsorption/desorption (Fig. 4). In addition, the colour variation, due to the adsorption–desorption of ethanol, was not changed in good correlation with the information obtained by PXRD patterns and SEM images.

Vapour (water and ethanol) sorption isotherms

Water and ethanol vapour sorption isotherms (Fig. 5) on HKUST-1 were measured gravimetrically at 303 K to understand the sorption performance of this microporous material. First, the water sorption isotherm was not reversible and the hysteresis was extended over the entire relative humidity range (0 to 90% RH). The total amount of water adsorbed by

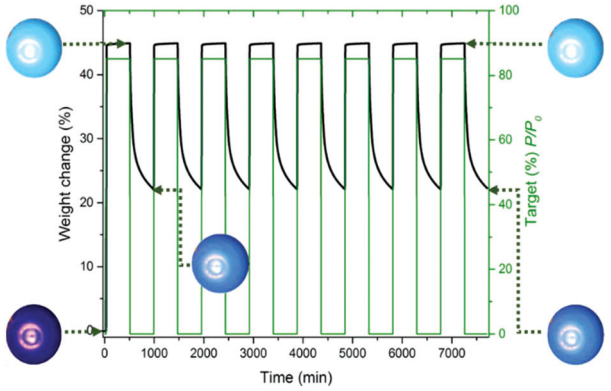

Fig. 4 Weight change variation through ethanol sorption cycle measurements at 303 K. Inset: *In situ* optical microscope images for colour changes of HKUST-1 in different steps of the cycle.

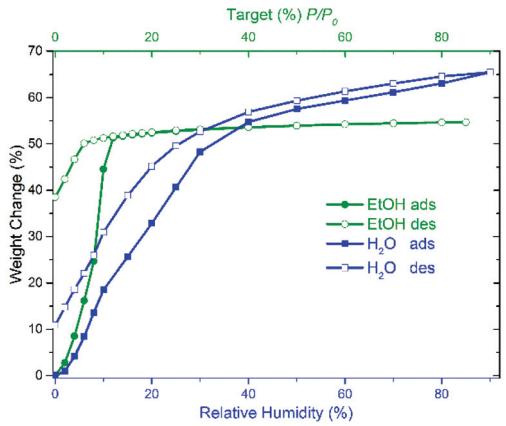

Fig. 5 Vapour sorption isotherms of water (blue) and ethanol (green) for HKUST-1 at 303 K.

HKUST-1 at 90% RH was equal to 36.4 mmol g^{-1}. The kinetics of the H_2O adsorbed material is initially better than in the work reported by DeCoste (32 mmol g^{-1}).[29] This can be rationalised due to the activation conditions; although DeCoste and co-workers[29] activated at the same temperature as us (423 K), they activated the HKUST-1 material for only 0.5 h, while we employed a time of 2 h. This time difference suggested that we managed to empty the MOF material more efficiently.

The water uptake increased continuously (adsorption) and the concave shape of the isotherm was attributed to the hydrogen-bonding which was formed by the adsorbed water molecules. Once the adsorption was completed, the desorption phase showed, as previously mentioned, a marked hysteresis and a remaining amount (10 wt%, see Fig. 5) of water was present within the material. Küsgens *et al.*[24] suggested that this final water residue, in the isotherm, was most likely water molecules chemisorbed (coordinated) to Cu(II) open sites.

Interestingly, the ethanol sorption isotherm was also not reversible with a maximum hysteresis loop at 0.02 P/P_0 and a total uptake of 11.9 mmol g^{-1} at P/P_0 of 0.85. This hysteresis loop, at low ethanol vapour partial pressure (<0.12 P/P_0), is a very clear indicator of a microporous sorbent. The ethanol isotherm rose steeply at low relative pressure with an asymptotic shape. Farha and Hupp[50] demonstrated that the adsorption of ethanol occurred by the coordination of the oxygen atom (from the hydroxyl group of the ethanol molecule) to the open Cu(II) sites of HKUST-1. The multilayer formation was poor due to weak hydrogen-bonding interactions from coordinated ethanol molecules with additional adsorbed ethanol molecules.

Up to this point, we have described the water and ethanol adsorption properties of HKUST-1. However, one of the main motivations, and nature, of this contribution is to provide additional information that could be very useful for some materials scientists. Although many efforts have been made to investigate the adsorption equilibrium in MOFs, diffusion analyses are considerably poor.[51] The relevance of diffusion coefficient determinations can be fully described by the possibility of calculating the diffusion selectivity of binary mixtures (an important task in membrane technology),[52] simulate breakthrough curves[35] and even characterize luminescence.[53] Thus, we estimated the diffusion coefficient for water and ethanol in HKUST-1. From a single adsorption kinetics curve, the solution for small multiples of the diffusion equation, considering a Fickian diffusion ($\mathcal{D}$), in which the isothermal flux is radial and the surface concentration is constant, the equation is equal to:[54]

$$\frac{M_t}{M_\infty} \cong \frac{6}{r_c}\sqrt{\frac{\mathcal{D}t}{\pi}} - \frac{3\mathcal{D}t}{{r_c}^2} \text{ for } \frac{M_t}{M_\infty} < 0.8 \quad (1)$$

where M_t/M_∞ is the ratio of the amount adsorbed in time t and the mass adsorbed at the infinite time (equilibrium adsorption mass). r_c is the crystal radius and $\mathcal{D}$ is the Fickian intracrystalline diffusion coefficient or diffusivity of the sorbate considered.[54] The crystal radius was estimated by the average particle radius measurement from the SEM images, assuming a set of uniform spherical particles, with the ImageJ program.[55]

For the as-received HKUST-1 sample, $\bar{r}_c$ (averaged crystal radius) was equal to 4.5 μm. Thus, by using eqn (1), we obtained $\mathcal{D}$ for water and ethanol, as 1.04 $m^2\ s^{-1}$ and 8.84 $m^2\ s^{-1}$, respectively, (Table 1). The values of the diffusivities for water and ethanol are a good approximation of their mobility within the pore structure of HKUST-1. Clearly, these results indicated that the ethanol diffusion, inside the micropores of the materials, is considerably higher than the diffusion of water. Indeed, the micropore diffusion, estimated from the gravimetric vapour (water and ethanol) sorption measure-

Table 1 Diffusivity, coefficient of determination and activation energy of diffusion for the vapour adsorption of water and ethanol onto HKUST-1 at 303 K

Sorbate	$\mathcal{D}$ (10^{-15}, $m^2\ s^{-1}$)	R^2 (%)	E_a (kJ mol^{-1})
Water	1.04	99.87	53.40
Ethanol	8.84	99.86	48.00

ments, can be rationalised as a consequence of the effect of concentration and pressure gradients (precisely, the diffusion driving force is the chemical potential gradient, which is related to concentration through the partial pressure of the sorbent[54]).

It is noteworthy that the partial pressure generated (by the sorption instrument) for each sorptive analyte (water and ethanol) is different. In order to establish a direct comparison of both kinetics curves (and therefore to compare the diffusion coefficients), the ethanol partial pressure to be considered (≈ 89.5 mbar) was indeed higher than the water partial pressure (≈ 38.2 mbar). Due to these boundary conditions, it is expected that ethanol diffuses faster than water in any experimental system.

To understand these results, it is necessary to analyse the pore dimensions of the MOF material. HKUST-1 is constructed from two different types of interconnected pores, two large pores with diameters of approximately 11 and 10 Å, and one micropore of 4 Å (diameter).[56] The collision diameters of water and ethanol (from the Stockmayer potential model) are 2.9 and 4.3 Å,[57] respectively. Thus, clearly water is sufficiently small to diffuse through all the porous of the HKUST-1 structure: the two large and relatively hydrophilic pores (11 Å and 10 Å) can be completely water-filled (due to affinity to open Cu(II) sites), and the small pores, although they are more hydrophobic, can be also reached by water since the collision diameter (2.9 Å) is smaller than this pore diameter (4 Å).

Conversely, ethanol could only have access to the two large micropores (10 and 11 Å) since its collision diameter (4.3 Å) is larger than the smallest micropore (4 Å). Thus, the ease of the ethanol diffusion (higher mobility) within the material can be attributed to the lower sorbent–sorbate interaction with Cu(II) open sites. In other words, these observations suggested that water is strongly adsorbed within HKUST-1, and its interaction energy is considerably higher than that between ethanol and uncoordinated Cu(II) sites. In order to corroborate this hypothesis, we calculated the binding energy (between sorbent and sorbate), thought to be the activation energy of diffusion E_a, which is a function of the dependence of diffusion coefficients on temperature, and it is empirically given by the Eyring equation:[58]

$$\mathcal{D}(T) = \mathcal{D}_0 \exp\left(-\frac{E_a}{kT}\right) \quad (2)$$

where $\mathcal{D}_0$ is the temperature-independent pre-exponential factor and k is the Boltzmann constant. By assuming a non-specific mechanism of the isotropic diffusion in a cF lattice, we obtained $\mathcal{D}_0 = 1/6a^2\nu$, where a is the distance of the stable jump positions and ν is the attempt frequency for sorbate molecules.[58]

In good agreement with the work of Zybaylo *et al.*,[59] we considered a = 1 nm and $\nu = 1 \times 10^{13}$ Hz (Debye vibration frequency) for HKUST-1. By using the diffusion coefficients previously determined at 303 K, we determined the binding energies of water (53.40 kJ mol^{-1}) and ethanol (48.00 kJ mol^{-1}) in HKUST-1 (Table 1). These energies represent the sorbate interaction with the open Cu(II) sites from the paddlewheel and they can be represented as:

$$\frac{1}{2}Cu_2(O_2CR)_4 + H_2O \rightleftharpoons \frac{1}{2}Cu_2(O_2CR)_4(H_2O)_2 \quad (3)$$

$$\frac{1}{2}Cu_2(O_2CR)_4 + 2C_2H_5OH \rightleftharpoons \frac{1}{2}Cu_2(O_2CR)_4(C_2H_5OH)_2 \quad (4)$$

where R represents the coordinated BTC ligand. Although the energies are relatively close (values), the E_a for water is higher than the energy of interaction for ethanol (see Table 1). These calculations corroborated our hypothesis (water is more strongly adsorbed than ethanol) and it was in good agreement with the computational calculations (*vide infra*).

Computational analyses

To further investigate the interactions between the sorbate molecules (ethanol and water) and the Cu(II) sites, a paddlewheel model was taken and we performed geometry optimisations and single point calculations. Optimised structures of both models (ethanol and water) are highly symmetric (see Fig. 6). Although the Cu–O bond distances were calculated to be very similar, the one for water was slightly larger (2.3 Å) than that for ethanol (2.2 Å).

The analysis of the atomic charges (Fig. S9, ESI†) indicated, as expected, that the metal atoms are positive (Cu(II)) and the surrounding oxygen atoms are negative. Interestingly, atomic charge values were calculated to be very similar for both systems (ethanol and water). However, the atomic charge of the hydrogen atom from the water (Fig. S9, ESI†) resulted to be more positive than the hydrogen atom from the ethanol. This result suggested that the hydrogen atom from water is more acidic than the one from ethanol. Of course, these results match perfectly with the current knowledge.

Sorbate stabilities

We have described and justified the different mobilities of water and ethanol within HKUST-1 as well as the sorbet interactions (calculations) with Cu(II) sites. Now, we aim to propose

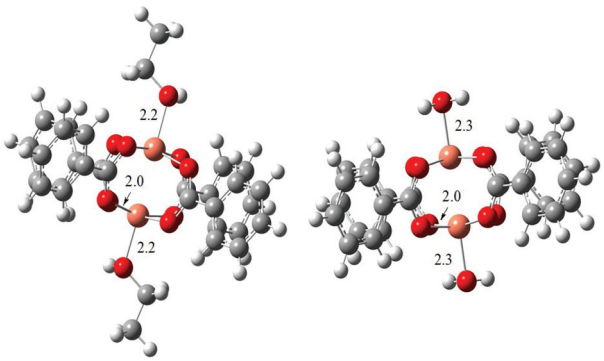

Fig. 6 Optimized structures of the models considering ethanol (left) and water (right) molecules. Representative bond distances (in Å) are emphasised. Colour keys: white (H), black (C), red (O) and pink (Cu).

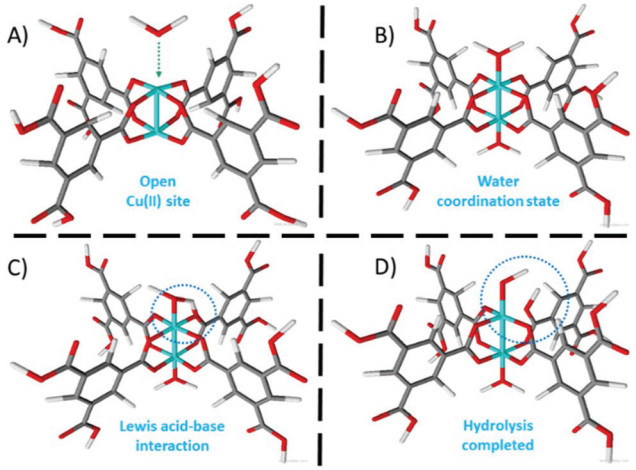

Fig. 7 A schematic representation of the square Cu_2 paddlewheel. (A) The unsaturated Cu(II) site. (B) Interaction with H_2O by coordination bonding. (C) Transition state where the acid proton of H_2O interacts with the oxygen from the BTC ligand. (D) Due to strong interaction, the Cu–O bond disrupts.

a plausible explanation for the water instability and ethanol stability of HKUST-1. The paddlewheel in HKUST-1, with a D_{4h} symmetry, is constructed by binuclear Cu(II) nodes and BTC ligands (see Fig. 7a).

Cu(II) cations have a d^9 configuration and their square planar geometry is stabilised *via* the Jahn–Teller effect.[60] The sorbate molecules (water and ethanol acting as Lewis bases) can link to the paddlewheel, axially (as shown by the computational analyses), by the formation of coordination bonds to Cu(II) cations (Lewis acid sites) (see Fig. 7b).

The coordination bond elongation due to the Jahn–Teller effect is expected to affect water and ethanol molecules equally (computational analyses). However, the acidity of the proton from the water molecule (analysis of the atomic charges) seems to play an essential structure-stability role. Thus, water disrupts the HKUST-1 framework by a slow but continuous hydrolysis of the symmetrical bidentate carboxylate ligands (with C–O bond equivalents) coordinated to binuclear Cu(II) cations (see Fig. 7c and d).

With a Brønsted–Lowry acidity nearly 80 times higher than ethanol (the pK_a for water is 14.0 while that for ethanol is 15.9 at 298 K), water is a better hydrogen-bonding donor. Thus, the transformation of the carboxylate group, linked to the Cu(II) cations, to the protonated acid equivalent occurs by an associative interchange mechanism (I_a).[61] The complete transformation of HKUST-1 to H_3BTC and $Cu(OH)_2$[29] did not take place but the PXRD pattern demonstrated partial degradation of the HKUST-1 structure (see Fig. 1). Based on the Bragg reflections ($2\theta \approx 9.1°$, 9.4°, 10.0°, 10.4°, 11.1° and 13.7°), the crystal structure of water-degraded HKUST-1 can correspond to two different phases: (i) a one-dimensional chain of a Cu:BTC coordination polymer ($2\theta \approx 9.0°$, 10.3°, 10.4° and 13.7°) and (ii) a layered structure of $[Cu_2OH(BTC)(H_2O)]$ ($2\theta \approx 9.4°$, 11.4°, 13.9° and 14.0°).[47] A very important and comprehensive mechanism was reported by Buscarino *et al.*[31] where they revealed the fundamental steps of the HKUST-1 hydrolysis. However, the formation of different phases was not included, due to the partial hydrolysis of the original structure, as Pérez-Ramírez[47] and our work suggest. Interestingly, these differences could be attributed to other variables (temperature, water load and aggregation state: liquid or vapour form) which afford different mechanistic routes.

Conversely, in the case of ethanol, its lower acidity and the weaker interaction with the open Cu(II) sites (binding energy) provide stability to the structure of HKUST-1 since the acid proton from the ethanol molecule does not break the Cu-carboxylate bond.

Carbon dioxide performance

After proposing a structural-stability explanation for HKUST-1 (when exposed to water and ethanol), we decided to investigate the CO_2 adsorption properties of this MOF material when small amounts of both solvents (water and ethanol) are confined within the micropores of HKUST-1. Then, isothermal and dynamic CO_2 adsorption experiments (kinetics) were carried out on desolvated HKUST-1. First, a sample of HKUST-1 was placed inside a thermobalance (Q500 HR) and activated by heating from room temperature to 423 K for 2 h and under a flow of pure N_2 gas. Later, the sample was cooled down to 303 K (under N_2). Finally, when the activated HKUST-1 sample reached 303 K, the N_2 purge flow was changed to 60 sccm of CO_2. Fig. 8 (anhydrous) shows the kinetics CO_2 uptake experiment at 303 K. At this temperature, the activated material showed the maximum weight percentage gain, which represents the maximum amount of CO_2 captured. This amount corresponds to approximately 12.9 wt%, which was rapidly reached after only 5 min and remained constant until the end of the experiment (12 min) (Fig. 8, Anhydrous).

Later, a sample of HKUST-1 was activated (423 K for 2 h and under a flow of N_2), cooled down to 303 K (under N_2) and saturated with EtOH (see Fig. S11, ESI†). After a specific activation protocol (see the ESI†) the residual amount of EtOH

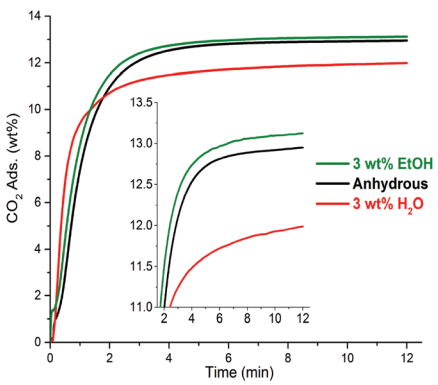

Fig. 8 Comparison of kinetics CO_2 uptake experiments performed in HKUST-1 with small loadings of pre-adsorbed water and ethanol at 303 K. Inset: Zoom of CO_2 adsorption emphasising the slightly enhanced CO_2 capture with the use of ethanol.

was equal to 3 wt%. Hereinafter, this sample will be referred as EtOH@HKUST-1. A similar procedure was carried out for the sample H_2O@HKUST-1 (see Fig. S10, ESI†).

We decided to use only pre-adsorbed small amounts of ethanol and water in HKUST-1 samples, based upon the following reasons: (i) Paesani and co-workers[62] showed by computational infrared spectroscopy that at low water loadings, these molecules can be perfectly accommodated within the pore walls of the microporous material MIL-53(Cr). Additionally, Maurin *et al.*[63] demonstrated by GCMC computational simulations, in the same MIL-53(Cr), how these H_2O molecules are regularly accommodated inside all the pores of the material. (ii) Relatively high amounts of water (as previously demonstrated by other research groups and ours) damaged the structure of HKUST-1, reducing considerably its capability to capture CO_2.

Thus, a kinetics CO_2 experiment, at 303 K, was performed on the EtOH@HKUST-1 sample. The maximum amount of CO_2 captured was equal to 13.1 wt%, which was achieved at approximately 5 min; it was constant until the end of the experiment (12 min) and it was improved by 0.2 wt% in comparison to anhydrous conditions, Fig. 8 (EtOH@HKUST-1).

In order to investigate if this slight CO_2 enhancement was due to the experimental error of the equipment, we decided to run 10 kinetics CO_2 uptake experiments on 10 different anhydrous HKUST-1 samples and 10 different EtOH@HKUST-1 samples. The results are shown in Table S1 (see the ESI†). The average maximum CO_2 uptakes were 12.905 wt% (anhydrous HKUST-1) and 13.103 wt% (EtOH@HKUST-1), demonstrating a CO_2 capture enhancement due to the presence of confined EtOH within the micropores of HKUST-1. Samples of EtOH@HKUST-1 were prepared using anhydrous ethanol (<0.005% water). Different small residual-amounts of ethanol were used (Fig. S11, ESI†) and the optimal result was achieved with 3 wt% of ethanol.

Then, the sample H_2O@HKUST-1 was synthesised (activation protocol, see the ESI†). The quantity of pre-adsorbed ethanol was equal to 3 wt%. In Fig. 8, the experiment (kinetics CO_2) is shown for H_2O@HKUST-1 where the maximum CO_2 captured was equal to 12.0 wt%. This amount (CO_2 uptake) was smaller in comparison to the samples HKUST-1 and EtOH@HKUST-1, suggesting that the incorporation of small amounts of ethanol in HKUST-1 retains and even increases the overall capture of CO_2.

On the other hand, the pre-adsorption of small amounts of water (even only 3 wt%) reduces the CO_2 capture capability of HKUST-1. The regeneration capacity (long-term) is a very important factor when a material is considered for CO_2 capture applications. Preferably, this regeneration capacity should exhibit low energy requirements when CO_2 is released from the capture material.[64] Typically, in many industrial CO_2 separation processes, this stage is considerably expensive and time-consuming.[65] The most common regeneration-methodology is swing adsorption, which operates by applying vacuum and while the temperature is increased. Examples of this methodology were presented by Long and co-workers[66] who reported the regeneration of mmen-CuBTTri by switching the flow (15% CO_2 in N_2) to a pure N_2 stream followed by increasing the temperature up to 333 K. Denayer *et al.*[67] performed regeneration studies on NH_2-MIL-53 by purging (with a flow of N_2) this MOF material at 432 K.

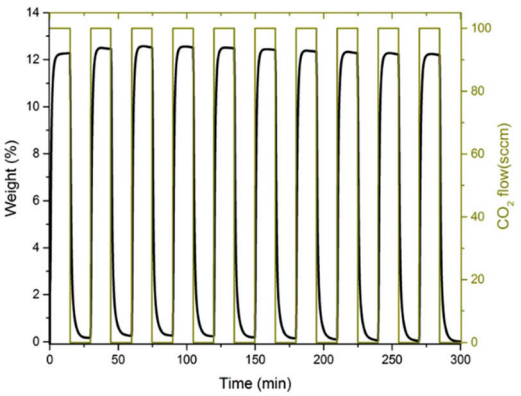

Fig. 9 CO_2 cycling measurements for the ethanol-impregnated HKUST-1 sample at 303 K, showing the reversibility of the capture process.

To evaluate the regeneration capacity of EtOH@HKUST-1, a fresh sample was synthesised (confining 3.1 wt% of EtOH within HKUST-1) and kinetics CO_2 adsorption–desorption experiments (cycling experiments at 303 K) were performed (Fig. 9). Each cycle is comprised of an adsorption step (15 min) and a desorption step (15 min), with a total cycling time of 30 min without the use of a N_2 purge or increasing the temperature.

The desorption step is achieved by turning off the CO_2 flow at 303 K. Interestingly, the complete regeneration of EtOH@HKUST-1 was accomplished without the need for a swing adsorption protocol. From the first cycle (12.3% CO_2 adsorption) to the tenth cycle, the CO_2 capacity was maintained with an average CO_2 capacity of 12.4 wt%. This regeneration capacity result for EtOH@HKUST-1 is remarkable since it was performed without purging (N_2) and no thermal re-activation of the sample was necessary, affording a very low energy-cost separation process.

Conclusions

HKUST-1, an unsaturated Cu(II) site MOF, showed some interesting characteristics when we compared the crystal structure stability after it was exposed to water and ethanol vapours. Although the water instability of HKUST-1 is well known, we have provided a chemical rationalisation of this behaviour through the comparative analysis of ethanol sorption. To the best of our knowledge, we proposed, for the first time, plausible mechanisms that explain the different structure stability of the HKUST-1 framework towards water and ethanol using diffusion coefficients and computational calculations. In our case, the structural degradation of HKUST-1 by slow hydrolysis

of Cu:BTC bonds is not complete; instead the framework transforms to a partially hydrolysed phase of lower symmetry. Although the water capacity was reduced, this material still has some degree of porosity as demonstrated by PXRD and BET surface area. Furthermore, we have also shown that the pre-adsorption of small amounts of ethanol (3 wt%, EtOH@HKUST-1) slightly enhanced CO_2 sorption in comparison with H_2O@HKUST-1 and anhydrous samples. Additionally, due to the reversibility of the CO_2 sorption process, the crystal structure of EtOH@HKUST-1 sample retained its crystallinity. Thus, these results show the potential use of alcohols like work fluids in CCS processes.

Acknowledgements

The authors acknowledge PAPIIT UNAM Mexico (IN100415) for financial support. E. G.-Z. acknowledge CONACyT (236879), Mexico, for financial support. Thanks to U. Winnberg (ITAM) for scientific discussions. A. I.-J. acknowledges the Departamento de Química CBI UAM-I for his position as a visiting professor (40966) and thanks J. Oscar C. Jiménez-Halla for his valuable comments. J. R. Á. acknowledges CONACyT Mexico (grant 276862); thanks also to Mayra D. Manrique-Ortega and M. Angélica García-Bucio for many useful discussions. E. S.-G. acknowledges CONACyT Mexico (Grant 289042).

Notes and references

1 S. R. Batten, N. R. Champness, X.-M. Chen, J. Garcia-Martinez, S. Kitagawa, L. Öhrström, M. O'Keeffe, M. Paik Suh and J. Reedijk, *Pure Appl. Chem.*, 2013, **85**, 1715–1724.
2 J. L. C. Rowsell and O. M. Yaghi, *Microporous Mesoporous Mater.*, 2004, **73**, 3–14.
3 H. Furukawa, K. E. Cordova, M. O'Keeffe and O. M. Yaghi, *Science*, 2013, **341**, 1–12.
4 N. MacDowell, N. Florin, A. Buchard, J. Hallett, A. Galindo, G. Jackson, C. S. Adjiman, C. K. Williams, N. Shah and P. Fennell, *Energy Environ. Sci.*, 2010, **3**, 1645.
5 B. Sreenivasulu, I. Sreedhar, P. Suresh and K. V. Raghavan, *Environ. Sci. Technol.*, 2015, **49**, 12641–12661.
6 M. Younas, M. Sohail, L. K. Leong, M. J. Bashir and S. Sumathi, *Int. J. Environ. Sci. Technol.*, 2016, **13**, 1839–1860.
7 J. Canivet, A. Fateeva, Y. Guo, B. Coasne and D. Farrusseng, *Chem. Soc. Rev.*, 2014, **43**, 5594–5617.
8 K. Tan, N. Nijem, Y. Gao, S. Zuluaga, J. Li, T. Thonhauser and Y. J. Chabal, *CrystEngComm*, 2015, **17**, 247–260.
9 A. M. Fracaroli, H. Furukawa, M. Suzuki, M. Dodd, S. Okajima, F. Gándara, J. A. Reimer and O. M. Yaghi, *J. Am. Chem. Soc.*, 2014, **136**, 8863–8866.
10 P. Li, J. Chen, J. Zhang and X. Wang, *Sep. Purif. Rev.*, 2014, **44**, 19–27.
11 E. Gonzalez-Zamora and I. A. Ibarra, *Mater. Chem. Front.*, 2017, DOI: 10.1039/C6QM00301J.
12 J. Wang, S. Wang, Q. Xin and Y. Li, *J. Mater. Chem. A*, 2017, **5**, 6794–6816.
13 A. C. Kizzie, A. G. Wong-Foy and A. J. Matzger, *Langmuir*, 2011, **27**, 6368–6373.
14 R. A. Peralta, B. Alcántar-Vázquez, M. Sánchez-Serratos, E. González-Zamora and I. A. Ibarra, *Inorg. Chem. Front.*, 2015, **2**, 898–903.
15 M. Sánchez-Serratos, P. A. Bayliss, R. A. Peralta, E. González-Zamora, E. Lima and I. A. Ibarra, *New J. Chem.*, 2016, **40**, 68–72.
16 J. R. Álvarez, R. A. Peralta, J. Balmaseda, E. González-Zamora and I. A. Ibarra, *Inorg. Chem. Front.*, 2015, **2**, 1080–1084.
17 E. Sánchez-González, J. R. Álvarez, R. A. Peralta, A. Campos-Reales-Pineda, A. Tejeda-Cruz, E. Lima, J. Balmaseda, E. González-Zamora and I. A. Ibarra, *ACS Omega*, 2016, **1**, 305–310.
18 S. S.-Y. Chui, S. M.-F. Lo, J. P. H. Charmant, A. G. Orpen and I. D. Williams, *Science*, 1999, **283**, 1148–1150.
19 M. Hartmann, S. Kunz, D. Himsl, O. Tangermann, S. Ernst and A. Wagener, *Langmuir*, 2008, **24**, 8634–8642.
20 S. Loera-Serna, M. A. Oliver-Tolentino, M. de Lourdes López-Núñez, A. Santana-Cruz, A. Guzmán-Vargas, R. Cabrera-Sierra, H. I. Beltrán and J. Flores, *J. Alloys Compd.*, 2012, **540**, 113–120.
21 Q. Min Wang, D. Shen, M. Bülow, M. Ling Lau, S. Deng, F. R. Fitch, N. O. Lemcoff and J. Semanscin, *Microporous Mesoporous Mater.*, 2002, **55**, 217–230.
22 S. Najafi Nobar and S. Farooq, *Chem. Eng. Sci.*, 2012, **84**, 801–813.
23 T. R. C. Van Assche, T. Duerinck, J. J. Gutiérrez Sevillano, S. Calero, G. V. Baron and J. F. M. Denayer, *J. Phys. Chem. C*, 2013, **117**, 18100–18111.
24 P. Küsgens, M. Rose, I. Senkovska, H. Fröde, A. Henschel, S. Siegle and S. Kaskel, *Microporous Mesoporous Mater.*, 2009, **120**, 325–330.
25 P. M. Schoenecker, C. G. Carson, H. Jasuja, C. J. J. Flemming and K. S. Walton, *Ind. Eng. Chem. Res.*, 2012, **51**, 6513–6519.
26 N. Al-Janabi, P. Hill, L. Torrente-Murciano, A. Garforth, P. Gorgojo, F. Siperstein and X. Fan, *Chem. Eng. J.*, 2015, **281**, 669–677.
27 J. M. Castillo, T. J. H. Vlugt and S. Calero, *J. Phys. Chem. C*, 2008, **112**, 15934–15939.
28 L. Grajciar, O. Bludský and P. Nachtigall, *J. Phys. Chem. Lett.*, 2010, **1**, 3354–3359.
29 J. B. DeCoste, G. W. Peterson, B. J. Schindler, K. L. Killops, M. a. Browe and J. J. Mahle, *J. Mater. Chem. A*, 2013, **1**, 11922.
30 F. Gul-E-Noor, B. Jee, A. Pöppl, M. Hartmann, D. Himsl and M. Bertmer, *Phys. Chem. Chem. Phys.*, 2011, **13**, 7783.
31 M. Todaro, G. Buscarino, L. Sciortino, A. Alessi, F. Messina, M. Taddei, M. Ranocchiari, M. Cannas and F. M. Gelardi, *J. Phys. Chem. C*, 2016, **120**, 12879–12889.
32 A. R. Millward and O. M. Yaghi, *J. Am. Chem. Soc.*, 2005, **127**, 17998–17999.

33 Z. Liang, M. Marshall and A. L. Chaffee, *Energy Fuels*, 2009, **23**, 2785–2789.
34 X. Yan, S. Komarneni, Z. Zhang and Z. Yan, *Microporous Mesoporous Mater.*, 2014, **183**, 69–73.
35 L. Hamon, E. Jolimaître and G. D. Pirngruber, *Ind. Eng. Chem. Res.*, 2010, **49**, 7497–7503.
36 K. Sumida, D. L. Rogow, J. A. Mason, T. M. McDonald, E. D. Bloch, Z. R. Herm, T.-H. Bae and J. R. Long, *Chem. Rev.*, 2012, **112**, 724–781.
37 A. Ö. Yazaydin, A. I. Benin, S. A. Faheem, P. Jakubczak, J. J. Low, R. R. Willis and R. Q. Snurr, *Chem. Mater.*, 2009, **21**, 1425–1430.
38 J. Liu, Y. Wang, A. I. Benin, P. Jakubczak, R. R. Willis and M. D. LeVan, *Langmuir*, 2010, **26**, 14301–14307.
39 H. Wu, Q. Gong, D. H. Olson and J. Li, *Chem. Rev.*, 2012, **112**, 836–868.
40 G. A. González-Martínez, J. A. Zárate, A. Martínez, E. Sánchez-González, J. R. Álvarez, E. Lima, E. González-Zamora and I. A. Ibarra, *RSC Adv.*, 2017, **7**, 24833–24840.
41 E. Sánchez-González, E. González-Zamora, D. Martínez-Otero, V. Jancik and I. A. Ibarra, *Inorg. Chem.*, 2017, **56**, 5863–5872.
42 F. Jeremias, D. Fröhlich, C. Janiak, S. K. Henninger, F. Jeremias, D. Fröhlich, C. Janiak and S. K. Henninger, *New J. Chem.*, 2014, **38**, 1846.
43 M. J. Frisch, et al., *Gaussian 09, Revision A.08*, Gaussian, Inc., Wallingford CT, 2009.
44 A. D. Becke, *J. Chem. Phys.*, 1993, **98**, 5648–5652.
45 C. Lee, W. Yang and R. G. Parr, *Phys. Rev. B: Condens. Matter*, 1988, **37**, 785–789.
46 M. P. Singh, N. R. Dhumal, H. J. Kim, J. Kiefer and J. A. Anderson, *J. Phys. Chem. C*, 2016, **120**, 17323–17333.
47 G. Majano, O. Martin, M. Hammes, S. Smeets, C. Baerlocher and J. Pérez-Ramírez, *Adv. Funct. Mater.*, 2014, **24**, 3855–3865.
48 C. Prestipino, L. Regli, J. G. Vitillo, F. Bonino, A. Damin, C. Lamberti, A. Zecchina, P. L. Solari, K. O. Kongshaug and S. Bordiga, *Chem. Mater.*, 2006, **18**, 1337–1346.
49 H. K. Kim, W. S. Yun, M. B. Kim, J. Y. Kim, Y. S. Bae, J. Lee and N. C. Jeong, *J. Am. Chem. Soc.*, 2015, **137**, 10009–10015.
50 N. C. Jeong, B. Samanta, C. Y. Lee, O. K. Farha and J. T. Hupp, *J. Am. Chem. Soc.*, 2012, **134**, 51–54.
51 S. Amirjalayer, M. Tafipolsky and R. Schmid, *Angew. Chem., Int. Ed.*, 2007, **46**, 463–466.
52 Z. Zhao, S. Wang, Y. Yang, X. Li, J. Li and Z. Li, *Chem. Eng. J.*, 2015, **259**, 79–89.
53 C. Wang and W. Lin, *J. Am. Chem. Soc.*, 2011, **133**, 4232–4235.
54 H. Mehrer, in *Diffusion in Solids: Fundamentals, Methods, Materials, Diffusion-Controlled Processes*, Springer, Berlin Heidelberg, 2007.
55 C. a. Schneider, W. S. Rasband and K. W. Eliceiri, *Nat. Methods*, 2012, **9**, 671–675.
56 D. Wu, X. Guo, H. Sun and A. Navrotsky, *J. Phys. Chem. C*, 2016, **120**, 7562–7567.
57 M. E. van Leeuwen, *Fluid Phase Equilib.*, 1994, **99**, 1–18.
58 A. Paul, T. Laurila, V. Vuorinen and S. V. Divinski, in *Thermodynamics, Diffusion and the Kirkendall Effect in Solids*, Springer International Publishing, Cham, 2014, pp. 167–238.
59 O. Zybaylo, O. Shekhah, H. Wang, M. Tafipolsky, R. Schmid, D. Johannsmann and C. Wöll, *Phys. Chem. Chem. Phys.*, 2010, **12**, 8092–8097.
60 S. Noro, *Phys. Chem. Chem. Phys.*, 2010, **12**, 2519–2531.
61 L. Helm and A. E. Merbach, *Chem. Rev.*, 2005, **105**, 1923–1959.
62 G. R. Medders and F. Paesani, *J. Phys. Chem. Lett.*, 2014, **5**, 2897–2902.
63 F. Salles, S. Bourrelly, H. Jobic, T. Devic, V. Guillerm, P. Llewellyn, C. Serre, G. Ferey and G. Maurin, *J. Phys. Chem. C*, 2011, **115**, 10764–10776.
64 R. A. Khatri, S. S. C. Chuang, Y. Soong and M. Gray, *Ind. Eng. Chem. Res.*, 2005, **44**, 3702–3708.
65 B. Metz, O. Davidson, H. de Coninck, M. Loos and L. Meyer, *IPCC Special Report: Carbon Dioxide Capture and Storage*, 2005.
66 T. M. McDonald, D. M. D'Alessandro, R. Krishna and J. R. Long, *Chem. Sci.*, 2011, **2**, 2022–2028.
67 S. Couck, J. F. M. Denayer, G. V. Baron, T. Rémy, J. Gascon and F. Kapteijn, *J. Am. Chem. Soc.*, 2009, **131**, 6326–6327.